ACS APPLIED MATERIALS & INTERFACES
Research Article
www.acsami.org

Graphene Quantum-Dot-Doped Polypyrrole Counter Electrode for High-Performance Dye-Sensitized Solar Cells

Lijia Chen,[†,‡] Chun Xian Guo,[†,‡] Qiaoming Zhang,[§] Yanlian Lei,[§] Jiale Xie,[†] Shujing Ee,[⊥] Guanhong Guai,[⊥] Qunliang Song,*[,†] and Chang Ming Li*[,†,⊥]

[†]Institute for Clean Energy & Advanced Materials and [§]School of Physical Science and Technology, Southwest University, Chongqing 400715, P.R. China

[⊥]Centre for Advanced Bionanosystems and School of Chemical and Biomedical Engineering, Nanyang Technological University, 70 Nanyang Drive, Singapore 637457, Singapore

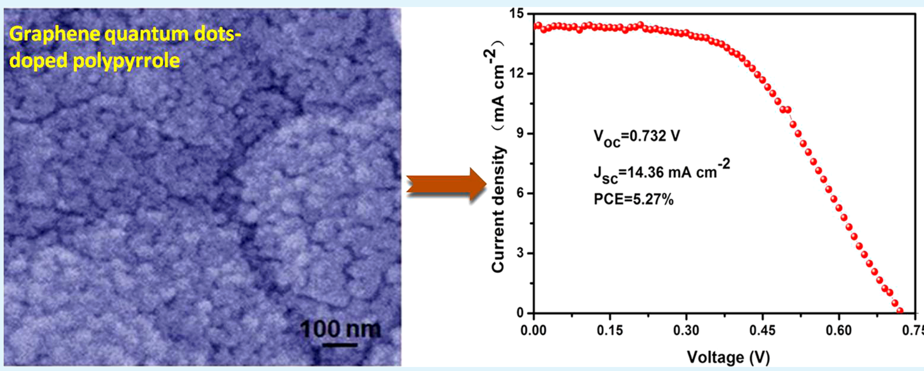

ABSTRACT: Herein graphene quantum dot (GQD), a graphene material with lateral dimension less than 100 nm, is explored to dope PPy on F-doped tin oxide glass as an efficient counter electrode for high-performance dye-sensitized solar cells (DSSCs). The GQDs-doped PPy film has a porous structure in comparison to the densely structured plain PPy, and displays higher catalytic current density and lower charge transfer resistance than the latter toward I_3^-/I^- redox reaction. The highest power conversion efficiency (5.27%) for DSSCs is achieved with PPy doped with10% GQDs, which is comparable to that of Pt counter electrode-based DSSCs. This work provides an inexpensive alternative to replace platinum for DSSCs.

KEYWORDS: *graphene quantum dots, polypyrrole, platinum-free counter electrode, dye-sensitized solar cell*

1. INTRODUCTION

Dye-sensitized solar cells (DSSCs) have fuelled up much attention because of their low manufacturing cost and high power conversion efficiency (PCE) recently.[1−6] A DSSC device consists of a dye-sensitized nanocryatalline-TiO_2 photoanode, electrolyte containing tri-iodide/iodide (I_3^-/I^-) redox couple, and a counter electrode (CE).[7,8] The TiO_2 photoanodes have been extensively studied,[9−11] whereas relatively less attention has been paid to the CE, which is also critical for the DSSC device performance because its sluggish kinetics could cause serious charge recombination at the photoelectrode, resulting in a low PCE.[12] Platinum (Pt) is considered to be the best CE material because of its high catalytic activity toward reducing I_3^- ions.[13−15] However, Pt is a noble metal and the high cost limits its practical application. It is of great importance to develop low-cost but well-performed CE. Conductive polymers have been recently applied as CE materials in DSSCs.[16−19] Among various conductive polymers, polypyrrole (PPy) is of great interest because of simple process, mass production, and low cost.[20−25] Nevertheless, its relatively high charge transfer resistance is the main barrier toward its practical applications.[26]

Graphene quantum dots (GQDs) are edge-bound nanometer-size graphene pieces with lateral dimensions less than 100 nm.[27] With the quantum confinement and edge effects, they exhibit unique electronic and optical properties,[28−31] and have been used for cell imaging, electrocatalysts, and light absorbers in photovoltaic devices.[32,33] Compared with carbon nanotubes and graphene, GQDs have much smaller sizes while retaining the graphitic nature. In this work, GQDs prepared with chemical oxidation approach were used to dope PPy via electrochemical codeposition method. The morphology and structure of prepared GQDs and GQD-doped PPy films on F-doped tin oxide (FTO) glass were characterized by field-emission scanning electron microscopy (FESEM) and transmission electron microscopes (TEM). The electrochemical properties of the GQD-doped PPy CEs were examined by cyclic voltammetry (CV) and electrochemical impedance spectroscopy (EIS). Effect of GQD doping percentage in the

Received: December 2, 2012
Accepted: February 28, 2013
Published: February 28, 2013

 © 2013 American Chemical Society

Scheme 1. Scheme of the Fabrication Processes of GQD-Doped PPy Film on FTO Glass and Its Application As a Counter Electrode in DSSCs

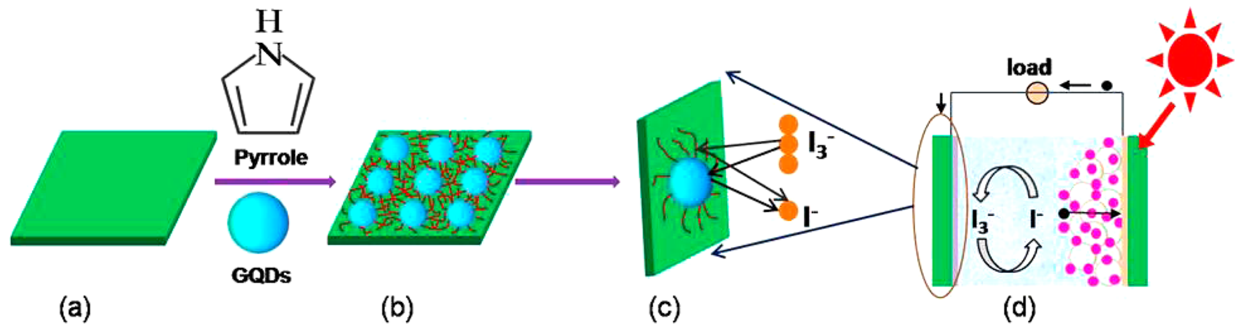

GQD-doped PPy film on the DSSC performance was investigated.

2. EXPERIMENTAL SECTION

2.1. Preparation of Counter Electrode. GQDs were synthesized via chemical oxidation approach. One-tenth of a gram of Vulcan XC-72 carbon black was put into 50 mL of 6 mol L^{-1} HNO_3 followed by refluxing overnight. After cooling to room temperature, the suspension was centrifuged. The supernatant was heated and a reddish-brown solid was obtained. Pyrrole (Py) solution was prepared by dispersing 65 μL distilled Py in 10 mL of 0.1 M lithium perchlorate ($LiClO_4$) solution. Different amounts of GQDs (weight ratio of GQDs:Py = 0, 3, 10, 15, 20, 25, and 30%) were added into the above Py solution. The electrochemical synthesis of polymer film has the advantage of a direct, low-cost, large area, and controllable synthesis on the surface of conducting substrates.[34] GQDs doped PPy on FTO glass were fabricated via electrochemical deposition method by setting a deposition voltage of 0.8 V (vs Ag/AgCl) for a certain of time. After electrodeposition, the GQD-doped PPy films were rinsed with deionized (DI) water and then dried at 80 °C under vacuum for 9 h. The fabrication process of GQDs doped PPy film is shown in Scheme 1. Pt sputtered on FTO glass was used as a control experiment for comparison with GQD-doped PPy films.

2.2. Preparation of TiO_2 Photoanodes. FTO glasses (Nippon Glass Sheet, ~12 Ω/□) were washed with detergent Dencon 90, DI water, acetone, and ethanol sequentially. The cleaned FTO glass was treated in 0.8 mM titanium(IV) fluoride (TiF_4) with 40% hydrofluoric acid (HF) at 70 °C for 30 min. The TiO_2 paste from DSL 18NR-T, Dyesol Co. was used for preparing 12 μm thick photoanode by doctor blade on FTO substrate. The TiO_2 films with an area of 0.1 cm^2 were dried in muffle furnace at 150 °C for 15 min, 275 °C for 15 min, then 350 °C for 10 min and finally sintered at 450 °C for 30 min. When the TiO_2 photoanodes were cooled down to 80 °C, they were socked in the 0.3 mM N719 (*cis*-diisothiocyanato-bis(2,2′-bipyridyl-4,4′-dicarboxylato)ruthenium(II)bis (tetrabutylammoni-um), Solaronix SA) dye solution mixing in a 1:1 volume of acetonitrile (Sigma-Aldrich) and tert-butanol (Sigma-Aldrich) for 16 h at room temperature. Dye-sensitized TiO_2 photoanodes were washed with acetonitrile and dried in air.

2.3. Fabrication of DSSCs. DSSCs were fabricated with a sandwiches structure by assembling the TiO_2 photoanode and CE. Then a drop of the iodide-based liquid electrolyte (HL-HPE, Dyesol Co.) was injected into the sandwiched cells through the drilled holes on the CEs. The DSSCs were finally sealed by parafilm. The distance between the CE and the photoanode is controlled by the parafilm with a thickness of 0.127 mm, which is good to prevent the electrical shorting. The effective area of the DSSCs is 0.1 cm^2.

2.4. Characterization of Materials and Investigation of DSSC Performance. The morphology and structure of the materials were investigated by transmission electron microscopy (TEM, JEM-2100 and JEM-2010F, Japan) and field emission scanning microscopy (SEM, JSM-6700F, Japan). Atomic force microscopy (AFM) image was obtained by a NanoscopeIIIa (Digital Instruments). Electrochemical characterizations were carried out by using CHI 660 D workstation with a three-electrode configuration with a Pt coil CE, a Ag/AgCl reference electrode and the GQDs doped PPy film working electrode. The electrolyte contains 9 mM lithium iodide (LiI), 1 mM I_2 and 0.1 M $LiClO_4$ in acetonitrile. Impedance curves were obtained under open-circuit voltage with a frequency range of 0.1 to 5 × 10^5 Hz at AC amplitude of 10 mV. The current−voltage (I−V) behaviors of DSSCs were measured with keithley 2420 source meter under 100 W cm^{-2} AM1.5G light illumination (550-W Xe source, Abet).

3. RESULTS AND DISCUSSION

TEM image in Figure 1a shows that the GQDs have a quite uniform size around 10 nm. AFM image together with the height profile tell that the GQDs have an average height of 0.8 nm, indicating its monolayer structure. SEM was used to examine the structure of GQD-doped PPy while using plain PPy as a control experiment with results shown in Figure 2. The GQDs-doped PPy film has a porous structure, whereas the plain PPy has a quite dense structure. It is known that conductive polymers have a chainlike structure and their electrodeposition via constant voltage can enable the connection of the polymerized film to the substrate. GQDs have abundant oxygen groups such as −COOH and −OH on

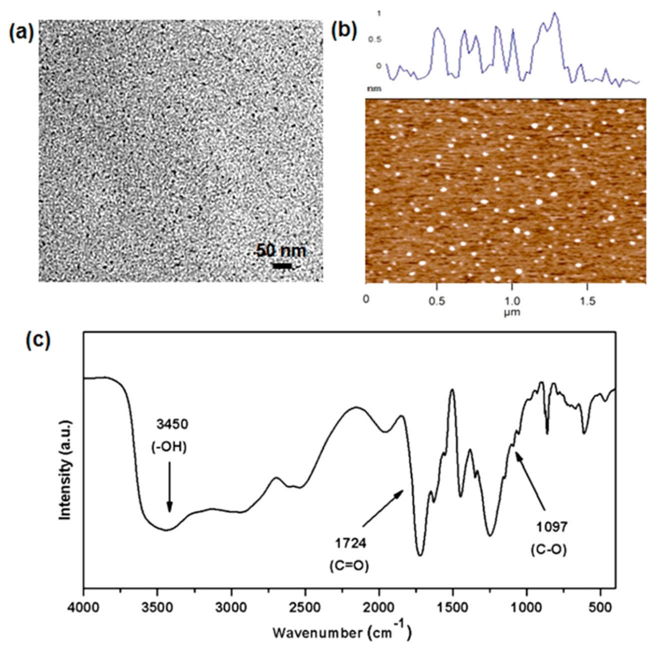

Figure 1. (a) TEM image, (b) AFM image with the corresponding height profile, and (c) FTIR spectrum of GQDs.

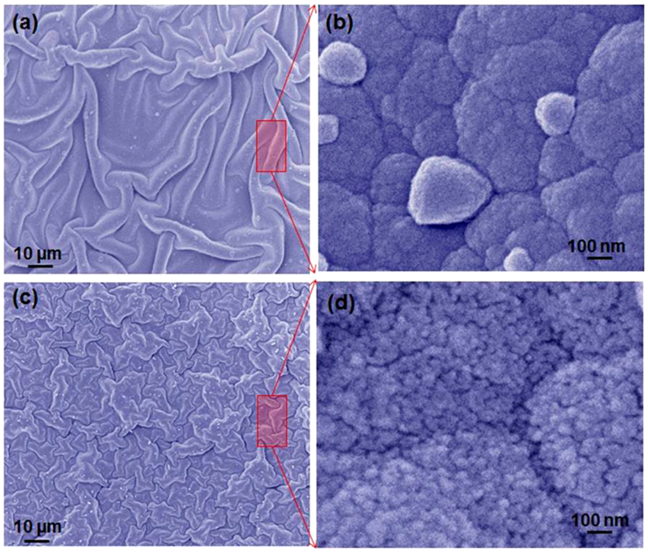

Figure 2. SEM images of (a, b) PPy and 10% GQD-doped (c, d) PPy with both low and high magnifications.

its edge,[29] as observed from the FITR spectrum shown in Figure 1c. Py molecule has positive charge in its N site[23] and should interact well with the negative charged GQDs. Thus, GQDs could electrostatically absorb Py as nucleation sites to promote the PPy growth, resulting in many "nano-islands" for a highly porous structure (Figure 2d). The more porous GQD-doped PPy counter electrode should increase electrocatalytic active centers and enhance reactant diffusion for better electrode kinetics and thermodynamics. More evidence for the success in incorporating GQDs into the PPy film is provided by the measured FTIR spectra. As shown in Figure 3,

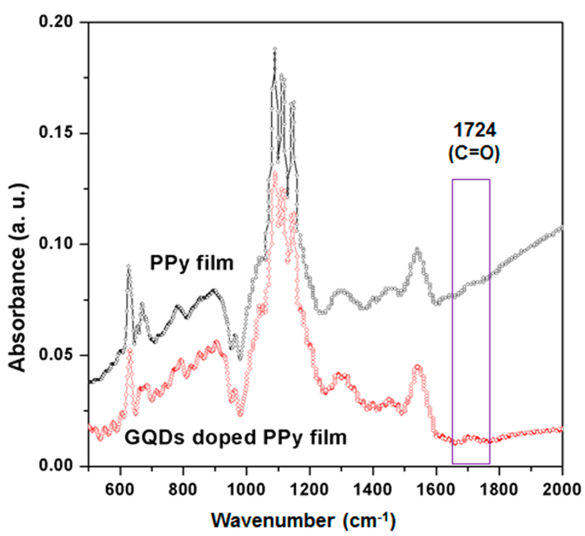

Figure 3. FTIR spectra of PPy film and 10% GQD-doped PPy film.

the GQD-doped PPy film exhibits a FTIR peak at 1724 cm^{-1} corresponding to C=O groups, which is observed in the plain GQDs as in Figure 1c and has been reported as the characteristic FTIR peak of GQDs.[29]

The electrocatalytic activities of GQDs doped PPy were examined by electrochemical characterizations. Figure 4a shows the CV curves of pristine PPy and GQDs doped PPy with a Pt (inset of figure 4a) CE at a scan rate of 20 mV s^{-1} in electrolyte

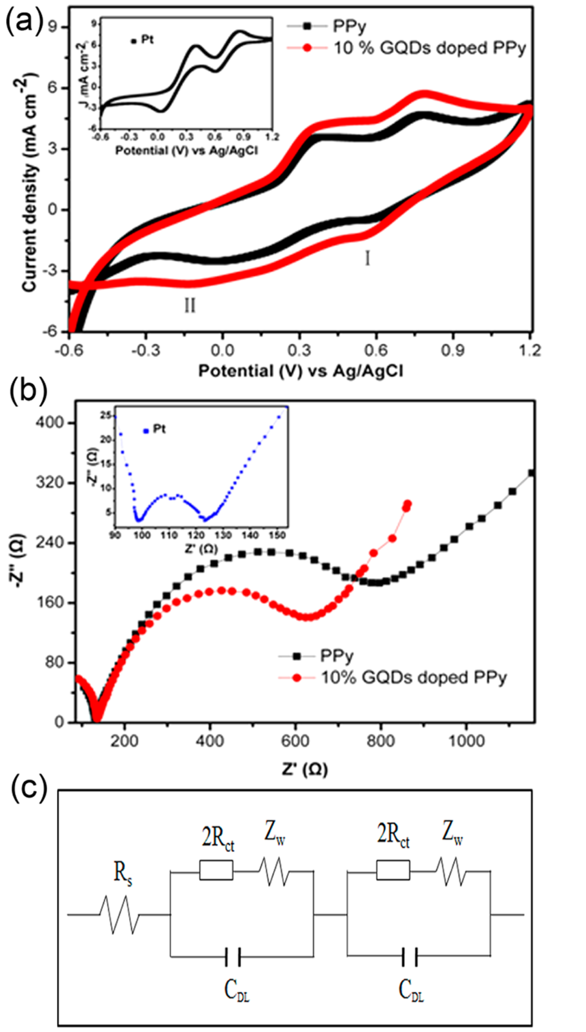

Figure 4. (a) CV curves of plain PPy counter electrode and GQD-doped PPy counter electrode at a scan rate of 20 mV s^{-1} in acetonitrile electrolyte containing 9 mM LiI, 1 mM I_2, and 0.1 M $LiClO_4$. The inset of a is CV of the Pt counter electrode. (b) Impedance spectra of plain PPy, and GQD-doped PPy CEs. The inset is the impedance spectrum of Pt CE. (c) Equivalent circuit for electrochemical impedance spectra shown in b, including a component R_s, series resistance; R_{ct}, charge transfer resistance; Z_w, Warburg impedance; and C_{DL}, capacitance of electric double layer.

containing 9 mM LiI, 1 mM iodine (I_2), 0.1 M $LiClO_4$ in acetonitrile solution. During DSSC operation, photoexcited electrons from dyes are injected into photoanode TiO_2 conduction band and the oxidized dyes are reduced by the I^- ion to I_3^- ions in the electrolyte. On the CE, the I_3^- ions are reduced on the surface. The reaction equations on the CE are as follows[35]

$$3I_2 + 2e^- \rightarrow 2I_3^- \qquad \text{(I)}$$

$$I_3^- + 2e^- \rightarrow 3I^- \qquad \text{(II)}$$

The electrochemical behaviors of GQD-doped PPy CE toward I^-/I_3^- redox reaction were examined in a three-electrode configuration by recording CV and EIS. The CVs in Figure 4a show typical one pair of adsorption peaks (~0.4 V vs Ag/AgCl) and one pair of the I^-/I_3^- redox reactions (at approximately −0.4 and 0.75 V) as the reported work.[36] The reduction peaks on GQD-doped PPy are more positive than the plain PPy and

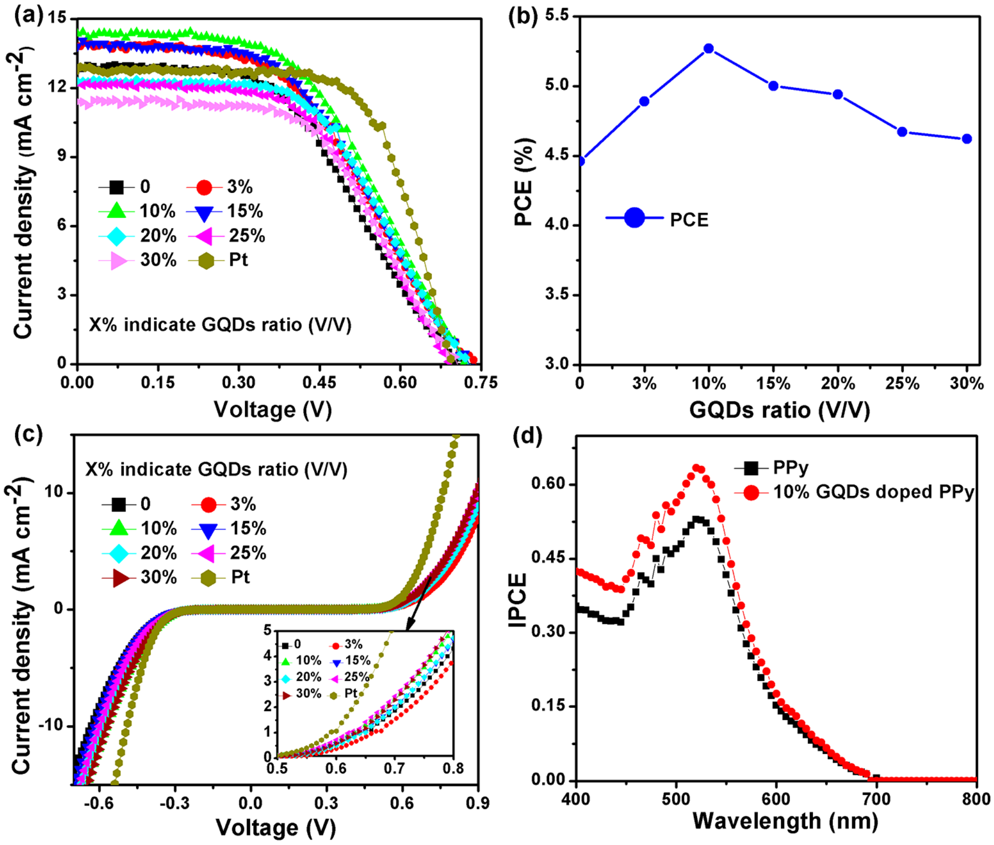

Figure 5. (a) $I-V$ curves of DSSCs based on Pt, plain PPy, and various concentrations GQDs ratio (3, 10, 15, 20, 25, and 30%) as CEs under AM1.5G light illumination of 100 mW cm^{-2}. (b) PCEs with different ratios of GQD-doped PPy as CEs for DSSCs. (c) $I-V$ curves of DSSCs based on Pt, plain PPy, and various GQD ratios (3, 10, 15, 20, 25, and 30%) as CEs under dark condition. The inset shows the enlarged curves in c for easy distinction. (d) IPCE spectrum of DSSCs with PPy and 10% GQDs doped PPy CEs.

the peak current densities are also higher than the latter, indicating that the former has higher electrocatalytic activity (more positive reduction peak) and more reaction active centers (high peak current) for reduction current of I_3^- ions. It is known that a larger enclosed redox reaction area of a CV curve represents a higher electrochemically active surface area of an electrode. Figure 4a displays that GQD-doped PPy CE has a higher electrochemically active surface area than plain PPy, which is consistent with that of SEM characterizations shown in Figure 2. One can also observe that the redox current density increases with increased GQDs content until to 10 wt %, then decreases (data not shown). The initial increased redox current density is very likely to be GQD-enabled porous PPy film (Figure 2d) for more active sites, achieving the best at 10 wt %, whereas more GQD incorporation could affect the polymerization process to reduce PPy active sites toward the I^-/I_3^- redox reaction. The film thickness is optimized by controlling the charge used for the electropolymerization, and 0.18 C charges provides the highest redox current density for GQDs doped PPy. It is noted that thicker GQD-doped PPy film easily falls off from FTO glass while resulting in higher resistance.

Figure 4b illustrates the Nyquist plots of GQD-doped PPy and PPy CEs. In the plots, the diameter of the semicircle represents the Faraday resistance of the electrochemical reaction. In an electrochemical reaction, a lower Faraday resistance indicates a faster electron transfer rate.[37] As shown in Figure 4b, the semicircle diameter of GQD-doped PPy CE is smaller than that of PPy CE, and decreases with increased GQD content up to 20%, followed by slightly decreasing. These results suggest that GQDs improve charge transfer rate of PPy during the cathodic reaction for higher electrocatalys is toward I^-/I_3^- redox reaction. The slope for the impedance spectrum in low frequency region related to reactant diffusion behavior is higher for GQD-doped PPy film than that of PPy, demonstrating GQD-doped PPy film is favorable to the reactant diffusion process. It is worthy of a note that the highest charge transfer rate observed by EIS is achieved by addition of 20% GQDs, whereas the highest peak current of the redox reaction is delivered by 10% GQD content. It is interesting that for both PPy and GQD-doped PPy film electrodes, a curve in the abscissa axis from 70 to 130 Ω is observed, which is likely resulted from the rough surface of the electrode, which has been also reported and explained with a given equivalent circuit as in Figure 4c.[38]

Figure 5a shows the $I-V$ curves for DSSCs made of TiO_2-dye photoelectrodes and CEs of Pt, PPy, and GQD-doped PPy with various GQDs concentrations (3, 10, 15, 20, 25, and 30%) under AM 1.5G light illumination of 100 mW cm^{-2}. The effect of GQDs concentration on the PCE of these DSSCs is given in Figure 5b. Important parameters including PCE, open-circuit voltage (V_{oc}), short-circuit current density (I_{sc}), and fill factor (FF) are summarized in Table 1. The results show that the PCE of DSSCs increases with the GQDs doping concentration up to 10% and then decreases with further GQDs incorporation. The highest PCE at 10% GQDs doping is 5.27% with the V_{oc} of 0.723 V, I_{sc} of 14.36 mA cm^{-2}, and FF of 50.8%, respectively, which is higher than that of plain PPy CE

Table 1. Performance (PCE, V_{oc}, I_{sc}, FF) List of DSSCs with Different CEs under AM1.5G Light Illumination

GQD ratio (V/V) (%)	PCE (%)	V_{oc} (V)	I_{sc} (mA cm^{-2})	FF (%)
0	4.46	0.715	12.83	48.6
3	4.89	0.740	13.81	47.9
10	5.27	0.723	14.36	50.8
15	5.00	0.728	13.80	49.8
20	4.94	0.726	12.23	55.6
25	4.67	0.700	12.07	55.6
30	4.62	0.705	11.41	57.3
Pt	6.02	0.696	12.81	67.5

(4.46%) by 20%. Table 1 shows that with increasing the GQD doping concentration, most parameters of the devices improve significantly, especially the I_{sc}, FF and PCE. The better I_{sc} with the GQD doping concentration should be corresponding to the small internal resistance.[39] Table 1 also indicates that the FF gradually increases as the increase of GQD content, which is very likely to be the faster electron charge transfer rate provided by the GQDs doping, as observed from the EIS in Figure 4b. Nevertheless, GQD-doped PPy with more GQDs could increase the charge recombination at photoelectrode because eof the slower reduction rate on the counter electrode,[37] resulting in decreased PCE. The measured IPCE spectra (Figure 5d) of DSSCs with PPy film and 10% GQDs doped PPy film show that the GQDs doping can enhance IPCE, which is consistent with the observation for the increased I_{sc}. These results clearly demonstrate that a proper amount of GQDs doping can significantly improve the performance of PPy CE-based DSSCs and GQD-doped PPy provides a promising candidate to replace Pt as CE for low-cost DSSCs.

4. CONCLUSIONS

In summary, GQDs were explored to dope PPy via an electrochemical codeposition method for fabricating GQDs-doped PPy as a counter electrode for DSSCs. GQD-doped PPy film has more porous structure, more active sites and higher charge transfer rate toward reduction of I_3^-/I^-. GQDs doping with 10% GQDs can greatly enhance the performance of DSSCs to achieve the highest PCE (5.27%), which is ~20% higher than that of plain PPy (4.46%) based DSSCs and is comparable to that of Pt counter electrode-based device (6.02%). The GQD-doped PPy provides a promising candidate to replace Pt as an inexpensive counter electrode for high-performance DSSCs.

AUTHOR INFORMATION

Corresponding Author

*E-mail: ecmli@ntu.edu.sg (C.M.L.); qunliang@gmail.com (Q.L.S.).

Author Contributions

‡C.X.G. and L.C. contributed equally to this work

Notes

The authors declare no competing financial interest.

ACKNOWLEDGMENTS

We gratefully acknowledge to the financial support from Institute for Clean Energy & Advanced Materials, Southwest University and Chongqing Key Laboratory for Advanced Materials and Technologies of Clean Energy, Chongqing Science and Technology Commission (cstc2012gjhz90002), P. R. China, the National Natural Science Foundation of China (Grants 10974159 and 11274256), the Chinese Ministry of Education under the Program for New Century Excellent Talents in Universities (Grants NCET-09-0659) and the Natural Science Foundation Project of CQ CSTC (2011BB6012). The project is also sponsored by SRF for ROCS, SEM, and the start-up Grant from Southwest University.

REFERENCES

(1) O'Regan, B.; Grätael, M. *Nature* **1991**, *353*, 737−740.

(2) Guai, G. H.; Li, Y.; Ng, C. M.; Li, C. M.; Chan-Park, M. B. *Chem. Phys. Chem.* **2012**, *13*, 2566−2572.

(3) Chen, T.; Guai, G. H.; Gong, C.; Hu, W.; Zhu, J.; Yang, H.; Yan, Q.; Li, C. M. *Energ. Environ. Sci.* **2012**, *5*, 6294−6298.

(4) Pang, H.; Yang, H.; Guo, C. X.; Lu, J.; Li, C. M. *Chem. Commun.* **2012**, *48*, 8832−8834.

(5) Yella, A.; Lee, H. W.; Tsao, H. N.; Yi, C. Y.; Chandiran, A. K.; Nazeeruddin, M. K.; Diau, E. W. G.; Yeh, C. Y.; Zakeeruddin, S. M.; Grätzel, M. *Science* **2011**, *334*, 629−634.

(6) Yue, G.; Lin, J. Y.; Tai, S. Y.; Xiao, Y.; Wua, J. *Electrochim. Acta* **2012**, *85*, 162−168.

(7) Yang, H.; Guai, G. H.; Guo, C.; Song, Q.; Jiang, S. P.; Wang, Y.; Zhang, W.; Li, C. M. *J. Phys. Chem. B* **2011**, *115*, 12209−12215.

(8) Lee, K. S.; Kwon, J.; Im, J. H.; Lee, C. R.; Park, N. G.; Park, J. H. *ACS Appl. Mater. Interfaces* **2012**, *4*, 4164−4168.

(9) Kay, A.; Grätzel, M. *Chem. Mater.* **2002**, *14*, 2930−2935.

(10) Sharmoukh, W.; Allam, N. K. *ACS Appl. Mater. Interfaces* **2012**, *4*, 4413−4418.

(11) Yang, Z.; Gao, S.; Li, T.; Liu, F.; Ren, Y.; Xu, T. *ACS Appl. Mater. Interfaces* **2012**, *4*, 4419−4427.

(12) Murakami, T. N.; Grätzel, M. *Inorg. Chim. Acta* **2008**, *361*, 572−580.

(13) Tjoa, V.; Chua, J.; Pramana, S. S.; Wei, J.; Mhaisalkar, S. G.; Mathews, N. *ACS Appl. Mater. Interfaces* **2012**, *4*, 3447−3452.

(14) Dao, V. D.; Kim, S. H.; Choi, H. S.; Kim, J. H.; Park, H. O.; Lee, J. K. *J. Phys. Chem. B* **2011**, *115*, 25529−25534.

(15) Jang, S. Y.; Kim, Y. G.; Kim, D. Y.; Kim, H. G.; Jo, S. M. *ACS Appl. Mater. Interfaces* **2012**, *4*, 3500−3507.

(16) Xia, J. B.; Masaki, N.; Jiang, K. J.; Yanagida, S. *J. Mater. Chem.* **2007**, *17*, 2845−2850.

(17) Li, Z. P.; Ye, B. X.; Hu, X. D.; Ma, X. Y.; Zhang, X. P.; Deng, Y. Q. *Electrochem. Commun.* **2009**, *11*, 1768−1771.

(18) Sudhagar, P.; Nagarajan, S.; Lee, Y. G.; Song, D.; Son, T.; Cho, W.; Heo, M.; Lee, K.; Won, J.; Kang, Y. S. *ACS Appl. Mater. Interfaces* **2011**, *3*, 1838−1843.

(19) Yue, G. T.; Wu, J. H.; Xiao, Y. M.; Lin, J. M.; Huang, M. L.; Lan, Z. *J. Phys. Chem. C* **2012**, *116*, 18057−18063.

(20) Zang, J.; Li, C. M.; Bao, S. J.; Cui, X.; Bao, Q.; Sun, C. Q. *Macromolecules* **2008**, *41*, 7053−7057.

(21) Li, C.; Sun, C.; Song, S.; Choong, V.; Maracas, G.; Zhang, X. *Front. Biosci.* **2005**, *10*, 180−186.

(22) Li, C.; Chen, W.; Yang, X.; Sun, C.; Gao, C.; Zheng, Z.; Sawyer, J. *Front Biosci.* **2005**, *10*, 2518−2526.

(23) Chen, W.; Lu, Z.; Li, C. M. *Anal. Chem.* **2008**, *80*, 8485−8492.

(24) Wu, J. H.; Li, Q. H.; Fan, L. Q.; Lan, Z.; Li, P. J.; Lin, J. M.; Hao, S. C. *J. Power Sources* **2008**, *181*, 172−176.

(25) Jeon, S. S.; Kim, C.; Ko, J.; Im, S. S. *J. Mater. Chem.* **2011**, *21*, 8146−8151.

(26) Keothongkham, K.; Pimanpang, S.; Maiaugree, W.; Saekow, S.; Jarernboon, W.; Amornkitbamrung, V. *Int. J. Photoenergy* **2012**, *2012*, 671326−611332.

(27) Peng, J.; Gao, W.; Gupta, B. K.; Liu, Z.; Romero-Aburto, R.; Ge, L.; Song, L.; Alemany, L. B.; Zhan, X.; Gao, G. *Nano Lett.* **2012**, *12*, 844−849.

(28) Gupta, V.; Chaudhary, N.; Srivastava, R.; Sharma, G. D.; Bhardwaj, R.; Chand, S. *J. Am. Chem. Soc.* **2011**, *133*, 9960−9963.

(29) Ponomarenko, L.; Schedin, F.; Katsnelson, M.; Yang, R.; Hill, E.; Novoselov, K.; Geim, A. *Science* **2008**, *320*, 356−358.
(30) Li, L.; Yan, X. *J. Phys. Chem. Lett.* **2010**, *1*, 21795−21800.
(31) Zhu, S. J.; Zhang, J. H.; Qiao, C. Y.; Tang, S. J.; Li, Y. F.; Yuan, W. J.; Li, B.; Tian, L.; Liu, F.; Hu, R.; Gao, H. N.; Wei, H. T.; Zhang, H.; Sun, H. C.; Yang, B. *Chem. Commun.* **2011**, *47*, 6858−6860.
(32) Guo, C. X.; Yang, H. B.; Sheng, Z. M.; Lu, Z. S.; Song, Q. L.; Li, C. M. *Angew. Chem., Int. Ed.* **2010**, *49*, 3014−3017.
(33) Yang, H. B.; Guo, C. X.; Guai, G. H.; Song, Q. L.; Jiang, S. P.; Li, C. M. *ACS Appl. Mater. Interfaces* **2011**, *3*, 1940−1945.
(34) Qin, Q.; Tao, J.; Yang, Y. *Synth. Met.* **2010**, *160*, 1167−1172.
(35) Peng, S. J.; Tian, L. L.; Liang, J.; Mhaisalkar, S. G.; Ramakrishna, S. *ACS Appl. Mater. Interfaces* **2012**, *4*, 397−404.
(36) Guai, G. H.; Song, Q. L.; Guo, C. X.; Lu, Z. S.; Chen, T.; Ng, C. M.; Li, C. M. *Sol. Energy* **2012**, *86*, 2041−2048.
(37) Guai, G. H.; Leiw, M. Y.; Ng, C. M.; Li, C. M. *Adv. Energy Mater.* **2012**, *2*, 334−338.
(38) Kaniyoor, A.; Ramaprabhu, S. *Electrochim. Acta* **2012**, *72*, 199−206.
(39) Peng, S. J.; Wu, Y. Z.; Zhu, P. N.; Thavasi, V.; Mhaisalkar, S. G.; Ramakrishna, S. *J. Photochem. Photobiol. A* **2011**, *223*, 97−102.